Atomic decay data for modeling the Al K lines[⋆]

P. Palmeri[1], P. Quinet[1,2], C. Mendoza[3], M. A. Bautista[4], J. García[5,6], M. C. Witthoeft[6], and T. R. Kallman[6]

1 Astrophysique et Spectroscopie (ASPECT), Université de Mons - UMONS, 20 Place du Parc, 7000 Mons, Belgium
  e-mail: patrick.palmeri@umons.ac.be
2 IPNAS, Université de Liège, Campus du Sart Tilman, Bât. B15, 4000 Liège, Belgium
  e-mail: pascal.quinet@umons.ac.be
3 Centro de Física, Instituto Venezolano de Investigaciones Científicas (IVIC), PO Box 20632, Caracas 1020A, Venezuela
  e-mail: claudio@ivic.gob.ve
4 Department of Physics, Western Michigan University, Kalamazoo, MI 49008, USA
  e-mail: manuel.bautista@wmich.edu
5 IACS-Department of Physics, The Catholic University of America, Washington, DC 20064, USA
  e-mail: javier@milkyway.gsfc.nasa.gov
6 NASA Goddard Space Flight Center, Greenbelt, MD 20771, USA
  e-mail: [michael.c.witthoeft;timothy.r.kallman]@nasa.gov

ABSTRACT

Radiative and Auger decay data have been calculated for modeling the K lines of the aluminum isonuclear sequence, from Al^0 up to Al^{11+}. Level energies, transition wavelengths, radiative transition probabilities, and radiative and Auger widths were determined using Cowan's Hartree-Fock with relativistic corrections (HFR) method. Results are compared with data sets computed with the AUTOSTRUCTURE and GRASP atomic structure codes and with available experimental and theoretical values, mainly in highly ionized ions and in the solid state.

Key words. atomic data – atomic processes – line: formation – X-rays: general

1. Introduction

The improved resolution and sensitivity of current satellite-borne X-ray telescopes (*Chandra*, *XMM Newton*, and *Suzaku*) are allowing study of weak spectral features which are nonetheless of astrophysical interest. This is the case for the aluminum K lines that have been observed in various astrophysical objects. For instance, the aluminum abundance in the hot interstellar medium of the elliptical galaxy NGC 4472 has been very recently determined from the analysis of *Suzaku* and *XMM Newton* spectra (Loewenstein & Davis 2010). The high-resolution *Chandra* spectrum of the micro quasar GRO J1655-40 has been analyzed, and the abundances of odd-*Z* elements, among them aluminum, have already been determined from the observed absorption K lines (Kallman et al. 2009). Al XIII and Al XII emission K lines were detected in high-resolution X-ray spectra of various clusters of galaxies recorded with the *XMM Newton* satellite (Peterson et al. 2003). Schulz et al. (2009) observed the prototype Z-source Cyg X-2 twice with *Chandra* at very high spectral resolution along its entire X-ray spectral variation pattern. The second strongest narrow (several hundred km s^{-1}) emission line was the He-like Al intercombination K line, detecting neither the resonance nor the forbidden line components. The Al XIII 1s−2p absorption line has been identified in the *Chandra* HETGS spectrum of the black hole candidate Cyg X-1, and may provide valuable

diagnostics on the physical condition of the stellar wind (Chang & Cui 2007). The coronal Al abundance of the eclipsing binary star AR Lacertae has been determined by Huenemoerder et al. (2003). They used the H- and He-like Al K lines detected in its high-resolution 97 ks spectrum recorded with the *Chandra* High Energy Transmission Grating spectrograph showing overabundance with respect to solar for this low first-ionization potential (FIP = 5.99 eV) element. A K-shell emission line of Al XII has also been identified in the high-resolution *Chandra* MEG spectrum of the nuclear region of the Seyfert 2 galaxy NGC 1068 (Ogle et al. 2003). Al is apparent in the spectra of several active stars observed by *XMM-Newton* and *Chandra* gratings (Nordon & Behar 2007), in the spectrum of the high mass X-ray binary Vela X-1 (Watanabe et al. 2006), the black hole candidate Cyg X-1 (Hanke et al. 2009), and in the highest signal-to-noise *Chandra* grating spectra from active galaxies, e.g., Kaspi et al. (2002) and Holczer et al. (2010).

Following the work by Palmeri et al. (2002, 2003a,b), Bautista et al. (2003, 2004), Mendoza et al. (2004), and Kallman et al. (2004) on the Fe K lines, by García et al. (2005) on the K-shell photoabsorption of O ions, by Palmeri et al. (2008a) on the Ne, Mg, Si, S, Ar, and Ca K lines, by Palmeri et al. (2008b) on the Ni K lines, and our recent studies of the K-shell photoionization and photoabsorption of N, Ne, Mg, Si, Ar, and Ca (García et al. 2009; Witthoeft et al. 2009), we report new atomic data for the K-vacancy levels in the aluminum isonuclear sequence. The main goals are to improve the atomic database of the XSTAR modeling code (Bautista & Kallman 2001) and to prepare ionic targets (configuration expansions and orbitals) for the lengthy computations of the K-shell photoabsorption and

---

⋆ Full Tables 14 and 15 are only available in electronic form at the CDS via anonymous ftp to
cdsarc.u-strasbg.fr (130.79.128.5) or via
http://cdsweb.u-strasbg.fr/viz-bin/qcat?J/A+A/525/A59

photoionization cross sections, where both radiative and Auger dampings are key effects (Palmeri et al. 2002).

Previous treatment of the K-shell structure of aluminum ions includes the one by Faenov et al. (1994) on satellites of the He-like ions resonance line in Al with electron number $4 \leq N \leq 9$. They measured wavelengths in a CO_2 laser-produced plasma and computed wavelengths, A-values, and Auger rates with the MZ implementation of the $1/Z$ expansion method (Vainshtein & Safronova 1978). Relativistic Auger and X-ray emission rates were calculated for states within the $1s2s^2$, $1s2s2p$, $1s2p^2$ configurations of Al XI and the $1s2p^6$ configuration of Al VII (Chen et al. 1981a,b, 1982) using the Dirac-Hartree-Slater (DHS) approach. A series of beam-foil spectroscopy (BFS) experiments were carried out in the eighties to measure the lifetimes of some K-vacancy states of He-like and Li-like aluminum ions (Armour et al. 1981; Buchet et al. 1984; Hellmann & Träbert 1985). Behar & Netzer (2002) used the relativistic multiconfiguration HULLAC code (Bar-Shalom et al. 2001) to calculate wavelengths, oscillator strengths, and total depletion rates for 1s-np transitions ($n \leq 3$) in ions of Al with $2 \leq N \leq 9$. Deslattes et al. (2003) have produced a comprehensive compilation of both measured and theoretical transition energies for K lines and edges in elements with $10 \leq Z \leq 100$. Recommended Al K line and Auger channel ratios and fluorescence yields were published by Schönfeld & Janssen (1996). Relative intensities of KLL Auger transitions in aluminum have been measured recently in the gas phase using the technique of Auger electron spectroscopy (Huttula et al. 2009). Gorczyca et al. (2003) audited the fluorescence database by Kaastra & Mewe (1993), which is widely used in modeling codes, in particular their scaling procedures along isoelectronic sequences. They found serious flaws that appear to compromise the application of this database in plasma modeling.

The outline of the present report is as follows. The numerical calculations are briefly described in Sect. 2, while an analysis of the results based on comparisons with previous experimental and theoretical values is carried out in Sect. 3. The two supplementary electronic tables are explained in Sect. 4, while some conclusions are finally discussed in Sect. 5.

2. Calculations

Three independent atomic structure packages were used. The main body of atomic data was computed with the Hartree-Fock with the relativistic corrections (HFR) method of Cowan (1981). Data accuracy was assessed by means of two other approaches: (i) the multiconfiguration Breit-Pauli method, which incorporates a scaled Thomas-Fermi-Dirac statistical potential as implemented in AUTOSTRUCTURE (Eissner et al. 1974; Badnell 1986, 1997); and (ii) the GRASP code (Grant et al. 1980; Grant & McKenzie, 1980; McKenzie et al. 1980) based on the multiconfiguration Dirac-Fock method.

In HFR and AUTOSTRUCTURE, wave functions are calculated with the Hamiltonian including the Breit-Pauli relativistic corrections

$$H_{BP} = H_{NR} + H_{1B} + H_{2B}, \qquad (1)$$

where H_{NR} is the usual nonrelativistic Hamiltonian. The one-body relativistic operators

$$H_{1B} = \sum_{n=1}^{N} f_n(\text{mass}) + f_n(D) + f_n(\text{so}) \qquad (2)$$

represent the spin-orbit interaction, $f_n(\text{so})$, the non-fine-structure mass variation, $f_n(\text{mass})$, and the one-body Darwin correction, $f_n(D)$. The two-body Breit operators are given by

$$H_{2B} = \sum_{n<m} g_{nm}(\text{so}) + g_{nm}(\text{ss}) + g_{nm}(\text{css}) + g_{nm}(D) + g_{nm}(\text{oo}), \quad (3)$$

where the fine-structure terms are $g_{nm}(\text{so})$ (spin-other-orbit and mutual spin-orbit) and $g_{nm}(\text{ss})$ (spin-spin), and the non-fine-structure counterparts are $g_{nm}(\text{css})$ (spin–spin contact), $g_{nm}(D)$ (two-body Darwin), and $g_{nm}(\text{oo})$ (orbit-orbit). HFR computes energies, A-values, and Auger rates with nonorthogonal orbital bases, which are generated by optimizing the average energy of each configuration. It also neglects the part of the Breit interaction (Eq. (3)) that cannot be reduced to a one-body operator. AUTOSTRUCTURE can use both orthogonal and nonorthogonal orbital bases for all the electronic configurations considered, which enables estimates of relaxation effects. Auger rates are computed in both HFR and AUTOSTRUCTURE in a distorted wave approach. The Auger decay channels considered in the present calculations and the configuration-interaction (CI) expansions used are the same as in our previous papers on the Fe isonuclear sequence (Bautista et al. 2003; Palmeri et al. 2003a,b, Mendoza et al. 2004).

Our third package is GRASP, which is an implementation of the multiconfiguration Dirac-Fock (MCDF) method where the atomic state function (ASF) is represented as a superposition of configuration state functions (CSF) of the type

$$\Psi(\alpha\Pi JM) = \sum_i c_i(\alpha)\Phi(\beta_i\Pi JM), \qquad (4)$$

where Ψ and Φ are the ASF and CSF, respectively; Π, J, and M are the relevant quantum numbers of parity, total angular momentum, and its associated total magnetic number, respectively; α and β_i stand for all the other quantum numbers that are needed to describe unambiguously the ASFs and CSFs. The summation in Eq. (4) is up to n_c, the number of CSFs in the expansion, and each CSF is built from antisymmetrized products of relativistic spin orbitals. The c_i coefficients, together with the orbitals, are optimized by minimizing an energy functional. The latter is built from one or more eigenvalues of the Dirac-Coulomb Hamiltonian depending on the optimization option adopted. In the present work, we have used the extended average level (EAL) option in which the $(2J + 1)$ weighted trace of the Hamiltonian is minimized. The transverse Breit interaction, as well as other QED interactions such as the vacuum polarization and self-energy, have been included in the Hamiltonian matrix as perturbations. The configuration expansions were limited to $n \leq 2$ for Al XII–Al V and to $n \leq 3$ for Al IV–Al I excluding the 3d subshell. This code does not treat the continuum, and has thus been exclusively employed in comparisons of radiative data for bound-bound transitions.

3. Results and discussions

Detailed comparisons with previous data have been carried out in order to obtain accuracy estimates and detect weak points. In the following sections, we give a concise account of our computations of level energies, K-vacancy state radiative, and Auger widths, as well as wavelengths and radiative transition probabilities for K lines in members of the Al isonuclear sequence denoted by electron number N. Some unresolved transition array (UTA) characteristics are studied in the second-row ions

$(10 \leq N \leq 13)$, namely the $\lambda_{K\alpha}$ and $\lambda_{K\beta}$ UTA centroid wavelengths, the Kβ/Kα line ratio, the KLM/KLL and KMM/KLL Auger channel ratios, and the K-shell fluorescence yield ω_K.

3.1. Energy levels

K-vacancy level energies for Al ions are very scarce in the literature. The NIST database (Ralchenko et al. 2008) lists values for He-, Li-, and Be-like aluminum that are interpolated or extrapolated from experimental level energies along isoelectronic sequences. Chen et al. (1981b) calculated values for the 1s2s2p configuration in Al^{10+} using the Dirac-Hartree-Slater (DHS) method. In Table 1, we compare our calculated level energies obtained with the three independent methods (HFR, AUTOSTRUCTURE, and MCDF) with the two above-mentioned data sets. In most cases, the agreement between the five data sets is better than 1 eV.

In Table 2, we present a comparison between the Al K-edge energies given in the compilation of Deslattes et al. (2003) for the solid, the gas phase, and the theory (the relativistic many body perturbation theory, RMBPT) with values determined by combining the first ionization potential given in the NIST database for Al I (IP = 5.985755 eV) with the energy of the lowest K-vacancy energy level in Al II obtained by our three methods. Here, all four calculations agree to within a few electronvolts with the gas phase experimental value. The HFR and the MCDF results are in close agreement and within 2 eV of the gas phase K-edge energy.

3.2. Wavelengths

Comparisons of wavelengths computed with our three independent methods are shown in Figs. 1–3. For the first-row ions $(2 \leq N \leq 9)$, good agreement between AUTOSTRUCTURE and HFR can be seen in Fig. 1 with an average wavelength difference of -1 ± 3 mÅ (error intervals hereafter correspond to one standard deviation, i.e. 68.33% confidence intervals). For these ions, our MCDF calculation predicts slightly longer wavelengths with an average difference of 7 ± 6 mÅ. In Fig. 2, the comparison is shown for the Kα lines of the second-row ions $(10 \leq N \leq 13)$. Both our AUTOSTRUCTURE and MCDF calculations predict slightly shorter wavelengths than HFR with average differences reaching -32 ± 2 and -27 ± 2 mÅ, respectively. The situation regarding the Kβ lines for these ions is somewhat different (see Fig. 3). The AUTOSTRUCTURE wavelengths are now marginally shorter than HFR with an average difference of -6 ± 4 mÅ, whereas MCDF wavelengths are in good agreement with HFR having an average difference of 0 ± 4 mÅ. Our HFR wavelengths agree with the values computed with HULLAC (Behar & Netzer 2002) to within a few mÅ except for the transitions listed in Table 3. This table compares our three models with the HULLAC calculation of Behar & Netzer (2002) for problematic HULLAC Al K line wavelengths. The HULLAC wavelength for the Li-like transition $1s^2 2s\ ^2S_{1/2} - 1s(^2S)2s2p(^3P^o)\ ^2P^o_{1/2}$ seems to be a misprint. The MCDF and HULLAC values for O-like and F-like ions suffer from the lack of relaxation effects.

In Table 4, for Al ions with $4 \leq N \leq 8$, the average wavelength differences with respect to the experimental (laser-produced plasma) values of Faenov et al. (1994), $\lambda_{\exp}$, are

compared with our three independent methods. This average is defined as

$$\overline{\Delta\lambda_e} = \frac{1}{M}\sum_{i=1}^{M}(\lambda^i_{calc} - \lambda^i_{exp}) \qquad (5)$$

where M is the number of classified lines. The absolute value of this quantity grows with the number of electrons, N, along the Al isonuclear sequence as already observed in the Ar isonuclear sequence (Palmeri et al. 2008a). Differences with HFR vary from $\overline{\Delta\lambda_e} = -3$ for $N = 4$ to $\overline{\Delta\lambda_e} = -24$ for $N = 8$, whereas those with AUTOSTRUCTURE and MCDF vary from $\overline{\Delta\lambda_e} = -5$ for $N = 4$ to $\overline{\Delta\lambda_e} = -22$ for $N = 8$ and from $\overline{\Delta\lambda_e} = 7$ for $N = 4$ to $\overline{\Delta\lambda_e} = -30$ for $N = 8$ respectively. As a result of the comparisons with the spectroscopic data, our calculated wavelengths for systems with $4 \leq N \leq 8$ have been empirically shifted with $-\overline{\Delta\lambda_e}$.

Comparisons of our computed UTA centroid wavelengths, $\lambda_{K\alpha}$ and $\lambda_{K\beta}$, for the second-row ions $(10 \leq N \leq 13)$ with the theoretical and experimental values of Deslattes et al. (2003), and the measurements of Lecherbourg et al. (2007) are presented in Table 5. The AUTOSTRUCTURE and MCDF $\lambda_{K\alpha}$ values are definitely too short, while our HFR value for $N = 12$ agrees remarkably well with the relativistic many-body pertubation theory (RMBPT) calculation of Deslattes et al. (2003) and is slightly shorter (by $\sim$5 mÅ) than the measurement compiled by the same authors. Lecherbourg et al. (2007) observed a broad line at 8.331 Å close to our HFR UTA centroid value of 8.329 Å but $\sim$30 mÅ longer than our AUTOSTRUCTURE (8.300 Å) and MCDF (8.301 Å) UTA centroid values. Regarding the Kβ UTA centroid wavelengths also shown in Table 5, a good agreement is observed for $N = 12$ between our HFR and MCDF calculations and the RMBPT value of Deslattes et al. (2003), with AUTOSTRUCTURE 10 mÅ shorter and experiment (Deslattes et al. 2003) 20 mÅ longer. The Kβ line of Al III observed by Lecherbourg et al. (2007) at 7.885 Å can also be compared to our predictions: 7.880 Å (HFR), 7.876 Å (AUTOSTRUCTURE), and 7.872 Å (MCDF). The $\lambda_{K\alpha}$ and $\lambda_{K\beta}$ trends along the second-row ions are significantly different between our three calculations, although they all increase with N. It may be appreciated that HFR better agrees with the experimental trends.

3.3. Transition probabilities and radiative widths

In Fig. 4, the ratios of the AUTOSTRUCTURE and HFR transition probabilities and those of MCDF and HFR are plotted as a function of the HFR A-values for the strong Al K lines, i.e. those with HFR A-values greater than or equal to 10^{13} s^{-1}, in all ions of the isonuclear sequence. Concerning AUTOSTRUCTURE, the average ratio is 0.99 ± 0.10, indicating a good accord with HFR for the strong lines. For MCDF, although the average A-value ratio is 0.97 ± 0.12 indicating fair agreement, two transitions in Be-like Al $(N = 4)$ and three transitions in C-like Al $(N = 6)$ have A-values that differ by more than 20% with respect to HFR. These transitions involve the K-vacancy states $1s(^1S)2s2p^{2,4}(^2D,^4P)\ ^3D_{1,2}$ and $^3P_{1,2}$ for which the LS compositions differ markedly between our two calculations. The corresponding comparisons for the radiative widths are shown in Fig. 5. The accord between AUTOSTRUCTURE and HFR is good with an average radiative width ratio of 0.99 ± 0.08, while the agreement between MCDF and HFR has deteriorated somewhat in the four Be-like $(N = 4)$ levels $1s(^1S)2s2p^2(^2D,^4P)\ ^3D_{1,2}$ and $^3P_{1,2}$ whose MCDF radiative widths differ by more than 20%

Table 1. K-vacancy level energies for Al ions with electron number $2 \leq N \leq 4$.

N	Level[b]	Energy (keV)				
		NIST[a]	HFR[b]	AS[c]	MCDF[d]	DHS[e]
2	$1s2s\ ^3S_1$	1.5749787	1.5745	1.5738	1.5724	
2	$1s2p\ ^3P^o_0$	1.5879705	1.5874	1.5871	1.5854	
2	$1s2p\ ^3P^o_1$	1.5881244	1.5877	1.5873	1.5856	
2	$1s2p\ ^3P^o_2$	1.5887598	1.5884	1.5879	1.5862	
2	$1s2s\ ^1S_0$	1.5889516	1.5890	1.5888	1.5870	
2	$1s2p\ ^1P^o_0$	1.5982902	1.5983	1.5978	1.5961	
3	$1s2s^2\ ^2S_{1/2}$	1.55717	1.5567	1.5568	1.5550	
3	$1s(^2S)2s2p(^3P^o)\ ^4P^o_{1/2}$	1.562848	1.5621	1.5623	1.5604	1.5618
3	$1s(^2S)2s2p(^3P^o)\ ^4P^o_{3/2}$	1.563041	1.5624	1.5625	1.5606	1.5620
3	$1s(^2S)2s2p(^3P^o)\ ^4P^o_{5/2}$	1.563524	1.5629	1.5629	1.5611	1.5624
3	$1s(^2S)2s2p(^3P^o)\ ^2P^o_{1/2}$	1.57963	1.5796	1.5800	1.5778	1.5793
3	$1s(^2S)2s2p(^3P^o)\ ^2P^o_{3/2}$	1.58003	1.5800	1.5804	1.5782	1.5797
3	$1s(^2S)2p^2(^3P)\ ^4P_{1/2}$	1.586065	1.5855	1.5857	1.5837	
3	$1s(^2S)2p^2(^3P)\ ^4P_{3/2}$	1.586389	1.5858	1.5860	1.5840	
3	$1s(^2S)2p^2(^3P)\ ^4P_{5/2}$	1.586748	1.5863	1.5863	1.5844	
3	$1s(^2S)2s2p(^1P^o)\ ^2P^o_{1/2}$	1.58753	1.5881	1.5887	1.5869	1.5882
3	$1s(^2S)2s2p(^1P^o)\ ^2P^o_{3/2}$	1.58772	1.5883	1.5888	1.5870	1.5884
3	$1s(^2S)2p^2(^1D)\ ^2D_{3/2}$	1.59687	1.5971	1.5977	1.5956	
3	$1s(^2S)2p^2(^1D)\ ^2D_{5/2}$	1.59673	1.5971	1.5975	1.5955	
3	$1s(^2S)2p^2(^3P)\ ^2P_{1/2}$	1.59961	1.5998	1.6001	1.5979	
3	$1s(^2S)2p^2(^3P)\ ^2P_{3/2}$	1.60029	1.6005	1.6008	1.5986	
3	$1s(^2S)2p^2(^1S)\ ^2S_{1/2}$	1.61215	1.6130	1.6135	1.6115	
4	$1s2s^22p\ ^3P^o_0$		1.5551	1.5555	1.5542	
4	$1s2s^22p\ ^3P^o_1$		1.5553	1.5556	1.5543	
4	$1s2s^22p\ ^3P^o_2$		1.5559	1.5561	1.5548	
4	$1s(^2S)2s2p^2(^4P)\ ^5P_1$		1.5591	1.5592	1.5577	
4	$1s(^2S)2s2p^2(^4P)\ ^5P_2$		1.5594	1.5595	1.5580	
4	$1s(^2S)2s2p^2(^4P)\ ^5P_3$		1.5598	1.5598	1.5583	
4	$1s2s^22p\ ^1P^o_1$	1.56467	1.5649	1.5652	1.5637	
4	$1s(^2S)2s2p^2(^4P)\ ^3P_0$	1.57946	1.5797	1.5801	1.5781	
4	$1s(^2S)2s2p^2(^2D)\ ^3D_1$	1.57927	1.5798	1.5802	1.5783	
4	$1s(^2S)2s2p^2(^2D)\ ^3D_2$	1.57921	1.5798	1.5802	1.5785	
4	$1s(^2S)2s2p^2(^2D)\ ^3D_3$	1.57912	1.5799	1.5802	1.5787	
4	$1s(^2S)2s2p^2(^4P)\ ^3P_1$	1.57973	1.5801	1.5805	1.5789	
4	$1s(^2S)2s2p^2(^4P)\ ^3P_2$	1.58014	1.5805	1.5808	1.5790	
4	$1s(^2S)2s2p^2(^2S)\ ^3S_1$		1.5898	1.5899	1.5884	
4	$1s2p^3\ ^5S^o_2$		1.5922	1.5922	1.5905	
4	$1s(^2S)2s2p^2(^2D)\ ^1D_2$	1.59193	1.5931	1.5937	1.5919	
4	$1s(^2S)2s2p^2(^2P)\ ^3P_0$		1.5938	1.5945	1.5931	
4	$1s(^2S)2s2p^2(^2P)\ ^3P_1$		1.5941	1.5947	1.5934	
4	$1s(^2S)2s2p^2(^2P)\ ^3P_2$	1.59306	1.5945	1.5951	1.5937	
4	$1s(^2S)2s2p^2(^2P)\ ^1P_1$	1.6001	1.6017	1.6023	1.6007	
4	$1s(^2S)2s2p^2(^2S)\ ^1S_0$		1.6031	1.6036	1.6017	
4	$1s2p^3\ ^3D^o_1$	1.60484	1.6057	1.6064	1.6046	
4	$1s2p^3\ ^3D^o_2$	1.60483	1.6057	1.6064	1.6046	
4	$1s2p^3\ ^3D^o_3$	1.60465	1.6058	1.6063	1.6045	
4	$1s2p^3\ ^3S^o_1$		1.6098	1.6101	1.6081	
4	$1s2p^3\ ^1D^o_2$	1.61294	1.6145	1.6151	1.6133	
4	$1s2p^3\ ^3P^o_0$		1.6155	1.6162	1.6145	
4	$1s2p^3\ ^3P^o_1$		1.6155	1.6161	1.6144	
4	$1s2p^3\ ^3P^o_2$	1.6144	1.6157	1.6162	1.6146	
4	$1s2p^3\ ^1P^o_1$	1.62261	1.6244	1.6251	1.6233	

Notes. [a] NIST database (Ralchenko et al. 2008). Level energies are determined by interpolation or extrapolation of known experimental values. [b] HFR calculation (this work). [c] AUTOSTRUCTURE calculation (this work). [d] MCDF calculation (this work). [e] DHS calculation (Chen et al. 1981b).

Table 2. Comparison of Al K-edge energies for $N = 12$.

Method	K-Edge Energy (keV)
HFR[a]	1.5688
AS[b]	1.5708
MCDF[c]	1.5688
DETHE[d]	1.56956
SOLID[e]	1.559893(15)
GAS[f]	1.56702(80)

Notes. [a] HFR calculation (this work). [b] AUTOSTRUCTURE calculation (this work). [c] MCDF calculation (this work). [d] Theoretical (RMBPT) value given in Deslattes et al. (2003). [e] Solid state experimental value given in Deslattes et al. (2003). [f] Gas-phase experimental value given in Deslattes et al. (2003).
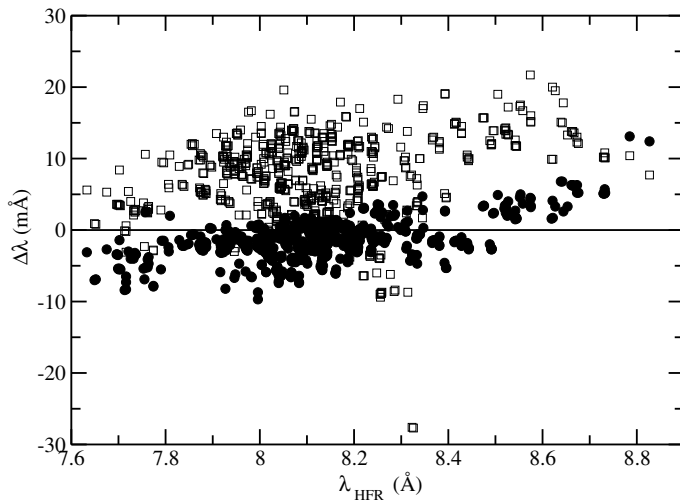

Fig. 1. Comparison of HFR wavelengths (in Å), λ_{HFR}, with AUTOSTRUCTURE and MCDF values for Al K lines in first-row ions ($2 \leq N \leq 9$). Wavelength differences (in mÅ), $\Delta\lambda$, with respect to HFR are plotted. The full circles and open squares represent differences between AUTOSTRUCTURE and HFR, and between MCDF and HFR, respectively. The straight line of equality has been drawn.

with HFR. Table 6 shows a comparison of the radiative parameters (A-values and radiative widths) for transitions involving these problematic K-vacancy levels. We compare two HFR calculations, the one described in Section 2 that includes the interactions with $n = 3$ configurations (HFR($n = 3$)) and a second where we excluded them (HFR($n = 2$)), with the MCDF calculation in which no $n = 3$ correlations have been considered. As one can see, the absence of correlations with $n = 3$ configurations in our MCDF calculation explains the differences with HFR($n = 3$).

A comparison between our radiative widths and those of Chen et al. (1981a,b, 1982) and of Vainshtein & Safronova (1978) is presented in Table 7 for ions with $N = 2, 3, 7$. The agreement among the five independent calculations is very good for widths greater than or equal to 10^{13} s^{-1}, the others being more model dependent.

3.4. Auger widths, total widths, and lifetimes

Figure 6 shows a comparison between our HFR and AUTOSTRUCTURE Auger widths for all the ions of the Al isonuclear sequence. Ratios of the HFR and
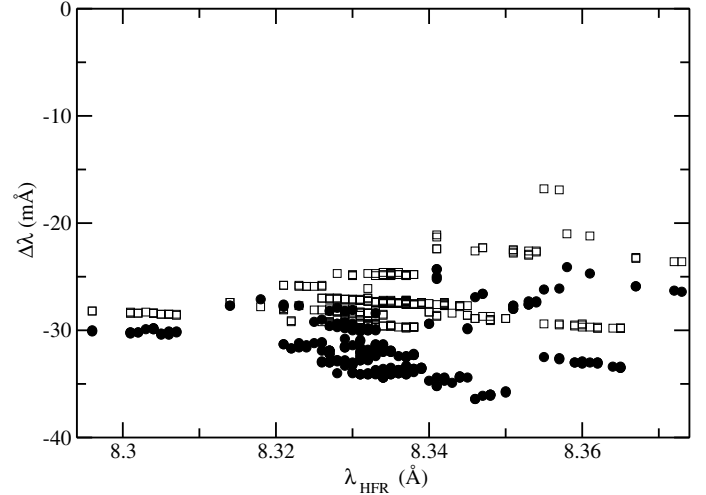

Fig. 2. Comparison of HFR wavelengths (in Å), λ_{HFR}, with AUTOSTRUCTURE and MCDF values for Al Kα lines in second-row ions ($10 \leq N \leq 13$). Wavelength differences (in mÅ), $\Delta\lambda$, with respect to HFR are plotted. The full circles and open squares represent differences between AUTOSTRUCTURE and HFR, and between MCDF and HFR, respectively.

Fig. 3. Comparison of HFR wavelengths (in Å), λ_{HFR}, with AUTOSTRUCTURE and MCDF values for Al Kβ lines in second-row ions ($10 \leq N \leq 13$). Wavelength differences (in mÅ), $\Delta\lambda$, with respect to HFR are plotted. The full circles and open squares represent differences between AUTOSTRUCTURE and HFR, and between MCDF and HFR, respectively. A straight line of equality has been drawn.
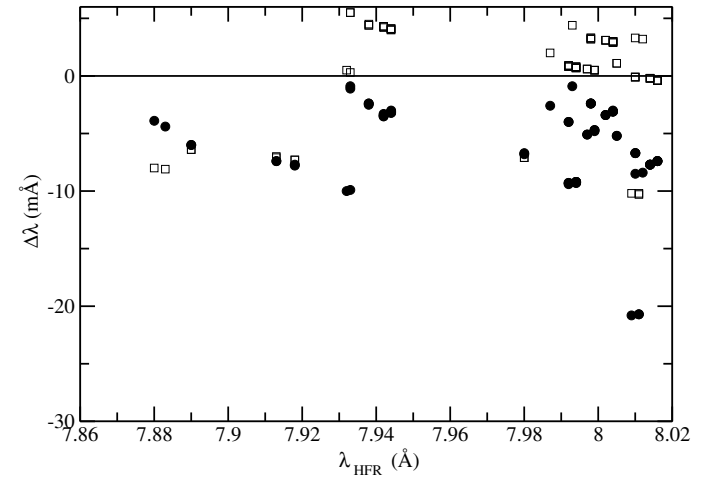
AUTOSTRUCTURE widths are plotted as a function of the HFR width for values of the latter greater than 10^{13} s^{-1}. A slight trend can be noticed where the AUTOSTRUCTURE values are higher with an averaged ratio of 1.06 ± 0.05.

In Table 8, a comparison between our Auger width values and those calculated by Chen et al. (1981a,b, 1982) and by Vainshtein & Safronova (1978) for $N = 3$ and 7 is displayed. As for the radiative widths, a good accord among the four independent calculations can be seen for values greater than or equal to 10^{13} s^{-1}, while the others are more model dependent.

We compare the total widths, i.e. the sum of the radiative and Auger widths, computed with HULLAC by Behar & Netzer (2002) with our HFR and AUTOSTRUCTURE values in Table 9. HULLAC total widths are systematically shorter with respect to both our data sets by up to a factor of 2 or more.

Table 3. Problematic HULLAC K line wavelengths.

N	Lower level	Upper level	λ(Å)			
			HFR[a]	AS[b]	MCDF[c]	HULLAC[d]
3	$1s^22s\ ^2S_{1/2}$	$1s(^2S)2s2p(^3P^o)\ ^2P^o_{1/2}$	7.849	7.847	7.858	7.486
8	$1s^22s^22p^4\ ^3P_2$	$1s2s^22p^5\ ^3P^o_2$	8.257	8.260	8.249	8.272
9	$1s^22s^22p^5\ ^2P^o_{1/2}$	$1s2s^22p^6\ ^2S_{1/2}$	8.323	8.320	8.296	8.337

Notes. [(a)] HFR calculation (this work). [(b)] AUTOSTRUCTURE calculation (this work). [(c)] MCDF calculation (this work). [(d)] HULLAC calculation (Behar & Netzer 2002).

Table 4. Average wavelength difference, $\overline{\Delta\lambda_e}$, with respect to the laser-produced plasma experimental wavelengths of Faenov et al. (1994) for Al ions with electron number $4 \leq N \leq 8$. The experimental error is 2 mÅ.

	$\overline{\Delta\lambda_e}^a$ (mÅ)		
N	HFR[b]	AS[c]	MCDF[d]
4	-3 ± 2	-5 ± 2	7 ± 2
5	-6 ± 3	-8 ± 3	2 ± 5
6	-9 ± 3	-11 ± 4	-3 ± 3
7	-15 ± 2	-16 ± 4	-14 ± 2
8	-24 ± 4	-22 ± 3	-30 ± 2

Notes. [(a)] In $a \pm b$, a is the actual average and b is the standard deviation. [(b)] HFR calculation (this work). [(c)] AUTOSTRUCTURE calculation (this work). [(d)] MCDF calculation (this work).
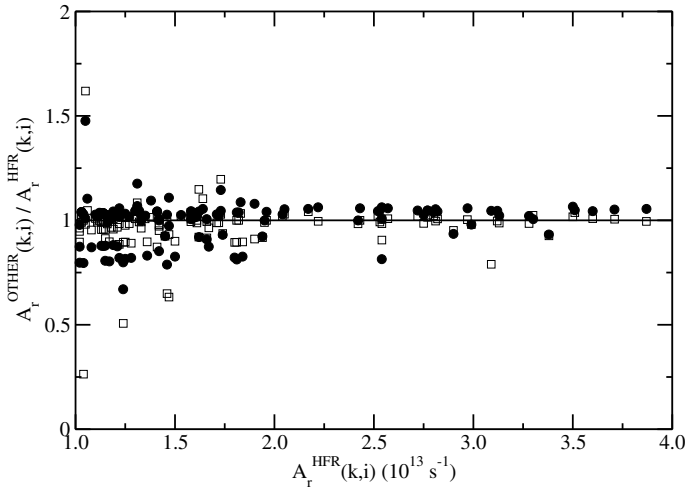

Fig. 4. Comparison of HFR transition probabilities (10^{13} s^{-1}), $A_r^{HFR}(k, i)$, with AUTOSTRUCTURE and MCDF values for strong Al K lines ($A_r(k, i) \geq 10^{13}$ s^{-1}). The A-value ratios, $A_r^{OTHER}(k, i)/A_r^{HFR}(k, i)$, with respect to HFR are plotted. The full circles and open squares represent AUTOSTRUCTURE and MCDF values, respectively. A straight line of equality has been drawn.

Fig. 5. Comparison of HFR radiative widths (10^{13} s^{-1}), $A_r^{HFR}(i)$, with AUTOSTRUCTURE and MCDF values. Widths greater than or equal to 10^{13} s^{-1} have been retained. The radiative width ratios, $A_r^{OTHER}(i)/A_r^{HFR}(i)$, with respect to HFR are plotted. The full circles and open squares represent AUTOSTRUCTURE and MCDF values, respectively. A straight line of equality has been drawn.
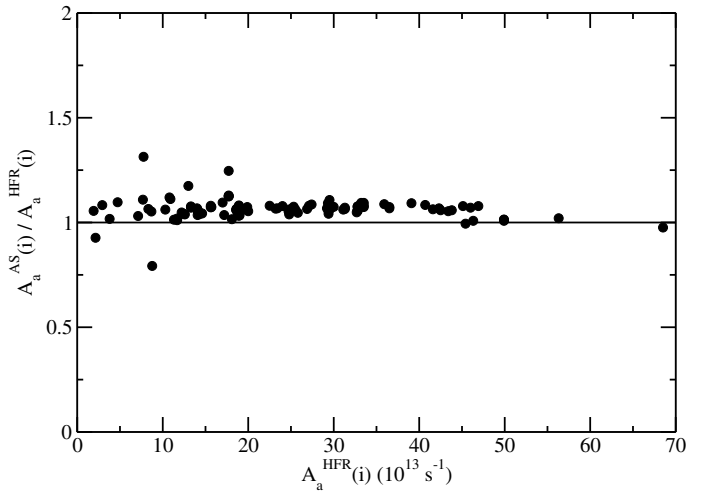
Fig. 6. Comparison of Auger widths (10^{13} s^{-1}), $A_a(i)$, calculated by HFR and AUTOSTRUCTURE (AS). Widths greater than or equal to 10^{13} s^{-1} have been retained. A straight line of equality has been drawn.

The available experimental lifetimes (Armour et al. 1981; Buchet et al. 1984; Hellmann & Träbert 1985) are compared to our predictions and to those of Chen et al. (1982) and Vainshtein & Safronova (1978) in Table 10. Our AUTOSTRUCTURE and MCDF predictions and those of Chen et al. (1982) agree reasonably well with the BFS lifetimes, whereas our HFR values for the $1s2p\ ^3P^o_1$ He-like and $1s(^2S)2p^2(^3P)\ ^4P_{3/2}$ Li-like levels are discrepant by up to a factor of $\sim$2. It was verified with AUTOSTRUCTURE that these states are particularly sensitive to the two-body Breit interactions that are missing from our HFR

model. In this respect, that the $1/Z$ value for the $1s(^2S)2p^2(^3P)$ $^4P_{3/2}$ level agrees with our HFR lifetime is puzzling, given that the $1/Z$ perturbation method is supposed to include these interactions.

The Kβ/Kα UTA line ratios computed with our three independent methods for Al ions with $10 \leq N \leq 13$ are

Table 5. UTA Kα and Kβ wavelengths for Al ions with electron number $10 \leq N \leq 13$.

N	$\lambda_{K\alpha}$ (Å)					$\lambda_{K\beta}$ (Å)				
	HFR[a]	AS[b]	MCDF[c]	DETHE[d]	EXP	HFR[a]	AS[b]	MCDF[c]	DETHE[d]	EXP
10	8.329	8.300	8.301		8.331[e]	7.880	7.876	7.872		7.885[e]
11	8.332	8.301	8.303			7.910	7.902	7.902		
12	8.335	8.301	8.310	8.3357	8.340286(58)[f]	7.939	7.929	7.940	7.9412	7.9601(30)[f]
13	8.336	8.303	8.309			7.942	7.940	7.948		

Notes. [a] HFR calculation (this work). The ab initio values are given. [b] AUTOSTRUCTURE calculation (this work). The ab initio values are given. [c] MCDF calculation (this work). The ab initio values are given. [d] Theoretical (RMBPT) value given in Deslattes et al. (2003). [e] Estimate from Fig. 6 of Lecherbourg et al. (2007). Spectral resolution ~10 mÅ. [f] Experimental value given in Deslattes et al. (2003).

Table 6. Comparison of HFR and MCDF radiative parameters for transitions involving problematic K-vacancy levels in Al ions with electron number $N = 4, 6$.

N	k	i	$A_r(k, i)$ (10^{13} s^{-1})		
			HFR($n = 3$)[a]	HFR($n = 2$)[b]	MCDF[c]
4	1s(^{1}S)2s2p^2(^{2}D) ^{3}D$_1$	1s^{2}2s2p ^{3}P$^o_0$	1.90	1.92	1.73
4		1s^{2}2s2p ^{3}P$^o_1$	0.02	0.38	0.55
4		1s^{2}2s2p ^{3}P$^o_2$	0.47	1.11	1.25
4	$A_r(k)$ (10^{13} s^{-1}) =		2.39	3.42	3.53
4	1s(^{1}S)2s2p^2(^{2}D) ^{3}D$_2$	1s^{2}2s2p ^{3}P$^o_1$	1.62	1.88	1.86
4		1s^{2}2s2p ^{3}P$^o_2$	0.02	0.36	0.67
4	$A_r(k)$ (10^{13} s^{-1}) =		1.64	2.24	2.53
4	1s(^{1}S)2s2p^2(^{4}P) ^{3}P$_1$	1s^{2}2s2p ^{3}P$^o_0$	0.07	0.09	0.22
4		1s^{2}2s2p ^{3}P$^o_1$	1.47	1.14	0.93
4		1s^{2}2s2p ^{3}P$^o_2$	1.04	0.45	0.27
4	$A_r(k)$ (10^{13} s^{-1}) =		2.59	1.69	1.42
4	1s(^{1}S)2s2p^2(^{4}P) ^{3}P$_2$	1s^{2}2s2p ^{3}P$^o_1$	0.26	0.03	0.0002
4		1s^{2}2s2p ^{3}P$^o_2$	3.09	2.84	2.44
4	$A_r(k)$ (10^{13} s^{-1}) =		3.35	2.88	2.44
6	1s(^{1}S)2s2p^4(^{4}P) ^{3}P$_1$	1s^{2}2s2p^3 ^{3}D$^o_2$	1.05	1.61	1.70
6		1s^{2}2s2p^3 ^{3}D$^o_1$	1.46	1.15	0.95
6		1s^{2}2s2p^3 ^{3}P$^o_0$	0.22	0.40	0.44
6		1s^{2}2s2p^3 ^{3}P$^o_1$	0.52	0.47	0.43
6		1s^{2}2s2p^3 ^{3}P$^o_2$	0.67	0.76	0.72
6		1s^{2}2s2p^3 ^{3}S$^o_1$	0.04	0.05	0.05
6	$A_r(k)$ (10^{13} s^{-1}) =		3.97	4.45	4.29
6	1s(^{1}S)2s2p^4(^{2}D) ^{3}D$_1$	1s^{2}2s2p^3 ^{3}D$^o_2$	1.23	0.83	0.63
6		1s^{2}2s2p^3 ^{3}D$^o_1$	0.49	0.93	1.02
6		1s^{2}2s2p^3 ^{3}P$^o_0$	0.60	0.45	0.37
6		1s^{2}2s2p^3 ^{3}P$^o_1$	0.02	0.09	0.12
6		1s^{2}2s2p^3 ^{3}P$^o_2$	0.06	0.006	0.0004
6	$A_r(k)$ (10^{13} s^{-1}) =		2.42	2.30	2.14

Notes. [a] HFR calculation including the interactions with $n = 3$ configurations (this work). [b] HFR calculation excluding the interactions with $n = 3$ configurations (this work). [c] MCDF calculation (this work).

compared with the recommended value of Schönfeld & Janssen (1996) in Table 11. MCDF values are systematically in between those of HFR and AUTOSTRUCTURE, with HFR ratios the lowest values. Scatters between MCDF and HFR vary from 19% for $N = 10$ to 14% for $N = 13$. Regarding HFR and AUTOSTRUCTURE, they vary from 29% for $N = 10$ to 39% for $N = 13$. For Al$^+$ ($N = 12$), the AUTOSTRUCTURE ratio is within the error bar of the recommended value of Schönfeld & Janssen (1996), with MCDF just outside and HFR within 2 standard deviations.

In Table 12, HFR relative intensities of KLL Auger transitions in Al$^+$ ($N = 12$) and in Al^{2+} ($N = 11$) are reported. The experimental values have been obtained from the KLL Auger electron spectrum recorded recently by Huttula et al. (2009) in the gas phase. A good agreement is observed between HFR and experiment.

Table 7. Comparison of radiative widths, A_r, of some K-vacancy levels in Al ions with electron number $N = 2, 3, 7$.

N	Level	A_r (s^{-1})[a]				
		HFR[b]	AS[c]	MCDF[d]	DHS[e]	1/Z[f]
2	$1s2p\ ^3P^o_0$	1.37(8)	1.55(8)	1.43(8)	–	–
2	$1s2p\ ^3P^o_1$	5.62(10)	7.11(10)	7.47(10)	–	7.32(10)
2	$1s2p\ ^3P^o_2$	1.71(8)	2.03(8)	1.71(8)	–	0
2	$1s2p\ ^1P^o_1$	2.99(13)	2.93(13)	2.93(13)	–	2.76(13)
3	$1s2s^2\ ^2S_{1/2}$	1.53(12)	1.72(12)	1.50(12)	1.19(12)	1.18(12)
3	$1s(^2S)2s2p(^3P^o)\ ^4P^o_{1/2}$	4.45(9)	6.37(9)	6.45(9)	6.33(9)	6.09(9)
3	$1s(^2S)2s2p(^3P^o)\ ^4P^o_{3/2}$	1.17(10)	1.64(10)	1.66(10)	1.63(10)	1.55(10)
3	$1s(^2S)2s2p(^3P^o)\ ^4P^o_{5/2}$	2.86(3)	–	1.20(5)	2.10(7)	0
3	$1s(^2S)2s2p(^3P^o)\ ^2P^o_{1/2}$	2.43(13)	2.57(13)	2.43(13)	2.41(13)	2.30(13)
3	$1s(^2S)2s2p(^3P^o)\ ^2P^o_{3/2}$	2.55(13)	2.70(13)	2.55(13)	2.53(13)	2.42(13)
3	$1s(^2S)2s2p(^1P^o)\ ^2P^o_{1/2}$	3.36(12)	3.48(12)	3.24(12)	3.51(12)	3.16(12)
3	$1s(^2S)2s2p(^1P^o)\ ^2P^o_{3/2}$	2.16(12)	2.17(12)	2.10(12)	2.30(12)	1.87(12)
3	$1s(^2S)2p^2(^3P)\ ^4P_{1/2}$	1.16(10)	1.32(10)	1.44(10)	1.27(10)	1.20(10)
3	$1s(^2S)2p^2(^3P)\ ^4P_{3/2}$	1.36(10)	1.86(10)	1.87(10)	1.67(10)	1.62(10)
3	$1s(^2S)2p^2(^3P)\ ^4P_{5/2}$	2.20(10)	2.28(10)	2.39(10)	2.31(10)	2.60(10)
3	$1s(^2S)2p^2(^1D)\ ^2D_{3/2}$	1.37(13)	1.41(13)	1.37(13)	1.36(13)	1.28(13)
3	$1s(^2S)2p^2(^1D)\ ^2D_{5/2}$	1.33(13)	1.36(13)	1.32(13)	1.32(13)	1.30(13)
3	$1s(^2S)2p^2(^3P)\ ^2P_{1/2}$	4.12(13)	4.30(13)	4.15(13)	3.96(13)	3.89(13)
3	$1s(^2S)2p^2(^3P)\ ^2P_{3/2}$	4.09(13)	4.26(13)	4.10(13)	3.92(13)	3.86(13)
3	$1s(^2S)2p^2(^1S)\ ^2S_{1/2}$	1.24(13)	1.31(13)	1.29(13)	1.19(13)	1.17(13)
7	$1s2p^6\ ^2S_{1/2}$	2.93(13)	2.92(13)	2.91(13)	3.04(13)	–

Notes. [a] $a(b)$ stands for $a \times 10^b$. [b] HFR calculation (this work). [c] AUTOSTRUCTURE calculation (this work). [d] MCDF calculation (this work). [e] DHS calculation (Chen et al. 1981a,b, 1982). [f] 1/Z calculation (Vainshtein & Safronova 1978).

Table 8. Comparison of Auger widths, A_a, of some K-vacancy levels in Al ions with electron number $N = 3, 7$.

N	Level	A_a (s^{-1})[a].			
		HFR[b]	AS[c]	DHS[d]	1/Z[e]
3	$1s2s^2\ ^2S_{1/2}$	1.22(14)	1.28(14)	1.27(14)	1.54(14)
3	$1s(^2S)2s2p(^3P^o)\ ^4P^o_{1/2}$	2.00(9)	5.05(9)	4.22(9)	6.28(9)
3	$1s(^2S)2s2p(^3P^o)\ ^4P^o_{3/2}$	6.00(9)	6.99(5)	1.18(8)	9.13(9)
3	$1s(^2S)2s2p(^3P^o)\ ^4P^o_{5/2}$	0	3.21(8)	3.34(8)	0
3	$1s(^2S)2s2p(^3P^o)\ ^2P^o_{1/2}$	8.94(12)	7.60(12)	3.35(13)	7.37(12)
3	$1s(^2S)2s2p(^3P^o)\ ^2P^o_{3/2}$	5.39(12)	3.45(12)	4.84(12)	3.36(12)
3	$1s(^2S)2s2p(^1P^o)\ ^2P^o_{1/2}$	8.31(13)	8.85(13)	8.81(13)	1.14(14)
3	$1s(^2S)2s2p(^1P^o)\ ^2P^o_{3/2}$	8.67(13)	9.12(13)	9.01(13)	1.18(14)
3	$1s(^2S)2p^2(^3P)\ ^4P_{1/2}$	1.00(9)	4.55(8)	4.83(8)	1.78(9)
3	$1s(^2S)2p^2(^3P)\ ^4P_{3/2}$	3.20(10)	4.99(9)	5.82(9)	2.53(10)
3	$1s(^2S)2p^2(^3P)\ ^4P_{5/2}$	2.22(11)	2.01(11)	2.09(11)	3.80(11)
3	$1s(^2S)2p^2(^1D)\ ^2D_{3/2}$	1.41(14)	1.46(14)	1.36(14)	1.84(14)
3	$1s(^2S)2p^2(^1D)\ ^2D_{5/2}$	1.43(14)	1.49(14)	1.39(14)	1.86(14)
3	$1s(^2S)2p^2(^3P)\ ^2P_{1/2}$	1.50(10)	1.31(10)	3.66(10)	2.00(10)
3	$1s(^2S)2p^2(^3P)\ ^2P_{3/2}$	1.91(12)	2.10(12)	1.84(12)	2.50(12)
3	$1s(^2S)2p^2(^1S)\ ^2S_{1/2}$	2.13(13)	1.98(13)	1.71(13)	2.64(13)
7	$1s2p^6\ ^2S_{1/2}$	4.75(14)	4.52(14)	4.92(14)	–

Notes. [a] $a(b)$ stands for $a \times 10^b$. [b] HFR calculation (this work). [c] AUTOSTRUCTURE calculation (this work). [d] DHS calculation (Chen et al. 1981a,b, 1982). [e] 1/Z calculation (Vainshtein & Safronova 1978).

Concerning the KLM/KLL and KMM/KLL Auger channel ratios, comparisons between HFR, AUTOSTRUCTURE and the recommended values of Schönfeld & Janssen (1996) are presented in Table 13. The HFR KLM/KLL ratio is right on the recommended value for $N = 12$, while the HFR KMM/KLL ratio is 2 standard deviations higher. Close accord is also found between the HFR and AUTOSTRUCTURE ratios except again

for the KMM/KLL ratio in the singly ionized species ($N = 12$), where the latter is now closer to the recommended value.

The K-shell fluorescence yields ω_K calculated by HFR and AUTOSTRUCTURE are also compared with the recommended value of Schönfeld & Janssen (1996) in Table 13. The accord between HFR and AUTOSTRUCTURE is very good with differences between 4% for $N = 10$ to 9% for $N = 13$, with

Table 9. Total widths, Γ_K, of some K-vacancy levels of Al ions with electron number $N = 2-9$.

N	Level	Γ_K (10^{13} s^{-1})		
		HFR[a]	AS[b]	HULLAC[c]
2	$1s2p\ ^2P^o_1$	2.99	2.93	2.56
3	$1s(^2S)2s2p(^3P^o)\ ^2P^o_{3/2}$	3.08	3.04	2.76
3	$1s(^2S)2s2p(^3P^o)\ ^2P^o_{1/2}$	3.32	3.33	3.05
4	$1s2s^22p\ ^1P^o_1$	13.0	13.7	10.6
5	$1s2s^22p^2\ ^2P_{1/2}$	14.5	15.9	6.19
5	$1s2s^22p^2\ ^2D_{3/2}$	28.3	30.6	21.9
6	$1s2s^22p^3\ ^3D^o_1$	34.6	37.1	30.8
6	$1s2s^22p^3\ ^3S^o_1$	17.2	19.5	9.58
7	$1s2s^22p^4\ ^4P_{5/2}$	37.5	40.2	34.8
8	$1s2s^22p^5\ ^3P^o_2$	51.8	52.4	40.2
9	$1s2s^22p^6\ ^2S_{1/2}$	58.9	59.9	47.7

Notes. [a] HFR calculation (this work). [b] AUTOSTRUCTURE calculation (this work). [c] HULLAC calculation (Behar & Netzer 2002).

Table 10. Comparison between calculated and experimental lifetimes, τ.

N	Level	τ(ps)					
		HFR[a]	AS[b]	MCDF[c]	DHS[d]	$1/Z$[e]	Exp.
2	$1s2p\ ^3P_1$	17.8	14.1	13.4		13.7	12.8 ± 0.7[f]
4	$1s(^2S)2p^2(^3P)\ ^4P_{1/2}$	79	73		76	73	69 ± 6[g]
							73 ± 8[h]
4	$1s(^2S)2p^2(^3P)\ ^4P_{3/2}$	22	42		45	24	38 ± 8[g]
4	$1s(^2S)2p^2(^3P)\ ^4P_{5/2}$	4	4		4	2	<5[g]

Notes. [a] HFR calculation (this work). [b] AUTOSTRUCTURE calculation (this work). [c] MCDF calculation (this work). [d] DHS calculation (Chen et al. 1982). [e] $1/Z$ calculation (Vainshtein & Safronova 1978). [f] BFS measurements (Armour et al. 1981). [g] BFS measurements (Hellman & Träbert 1985). [h] BFS measurements (Buchet et al. 1984).

HFR values systematically lower than AUTOSTRUCTURE. Although the HFR value for $N = 12$ is outside the error bar of the recommended yield by a little more than 3 standard deviations, the difference is less than 10%, while the discord with AUTOSTRUCTURE grows to 16%.

4. Supplementary electronic tables

Computed level energies, wavelengths, radiative transition probabilities, absorption oscillator strengths, radiative and Auger widths, and K-shell fluorescence yields in $Al^0 - Al^{11+}$ can be accessed electronically at the CDS via anonymous ftp to cdsarc.u-strasbg.fr (130.79.128.5) or via http://cdsweb.u-strasbg.fr/viz-bin/qcat?J/A+A/vol/page. The printed version shows data for ions with electron number $N \leq 3$.

It may be seen in Table 14 that levels are identified with the vector $(N, i, 2S+1, L, 2J, \text{Conf})$ where N is the electron number, i the level index, $2S+1$ the spin multiplicity, L the total orbital angular momentum quantum number, J the total angular momentum quantum number, and Conf the level configuration assignment. For each level, the computed HFR energy and its radiative width $A_r(i)$ are listed. For K-vacancy levels, the Auger width $A_a(i)$ and the K-shell fluorescence yield $\omega_K(i)$ are also given. In Table 15 transitions are identified with the vector (N, k, i) where k and i are the upper and lower level indices, respectively,

Table 11. UTA Kβ/Kα line ratio for Al ions with electron number $10 \leq N \leq 13$.

N	Kβ/Kα			
	HFR[a]	AS[b]	MCDF[c]	Rec[d]
10	0.0115	0.0163	0.0142	
11	0.0150	0.0233	0.0189	
12	0.0153	0.0222	0.0177	0.021(3)
13	0.0261	0.0426	0.0303	

Notes. [a] HFR calculation (this work). [b] AUTOSTRUCTURE calculation (this work). [c] MCDF calculation (this work). [d] Recommended value (Schönfeld & Janssen 1996).

Table 12. Relative intensities for KLL Auger transitions in Al ions with electron number $N = 11, 12$.

N	Transition[a]	Relative Intensity (%)	
		HFR[b]	EXP[c]
11	KL_1L_1	9	4
11	$KL_1L_{2,3}$	26	21
11	$KL_{2,3}L_{2,3}$	65	75
11	Σ	100	100
12	KL_1L_1	9	7
12	$KL_1L_{2,3}$	26	24
12	$KL_{2,3}L_{2,3}$	65	69
12	Σ	100	100

Notes. [a] L_1 and $L_{2,3}$ correspond to subshells 2s and 2p respectively. [b] HFR calculation (this work). [c] Experiment (Huttula et al. 2009).

tabulating its computed wavelength λ, radiative transition probability $A_r(k, i)$, weighted oscillator strength $gf(i, k)$, and cancelation factor CF as defined by Cowan (1981). The empirically shifted wavelengths are given for $4 \leq N \leq 8$ (see Sect. 3.2).

5. Summary and conclusion

Extensive data sets containing energy levels, wavelengths, radiative transition probabilities, absorption oscillator strengths, radiative and Auger widths, and fluorescence yields for K-vacancy levels in the aluminum isonuclear sequence have been computed with the atomic structure codes HFR, AUTOSTRUCTURE, and GRASP.

Comparisons of K-vacancy level energies calculated with our three independent methods with the few data available in the literature for $2 \leq N \leq 4$ (Ralchenko et al. 2008; Chen et al. 1981b) show an agreement better than 1 eV in most cases. Our calculated K-edge energies for $N = 12$ were also compared with the data given in Deslattes et al. (2003); they agree within a few electronvolts with the RMBPT and the gas-phase values reported in that compilation.

Concerning wavelengths, a good accord is found (within a few mÅ) between our three calculations for the first-row ions ($2 \leq N \leq 9$), while both AUTOSTRUCTURE and MCDF predict shorter wavelengths (by ~30 mÅ) than HFR for the Kα lines of second-row ions ($10 \leq N \leq 13$), but an accord of a few mÅ is held for the Kβ lines of these ions. As a result of the comparisons with the laser-produced plasma wavelengths

Table 13. UTA KLM/KLL and KMM/KLL ratios and K-shell fluorescence yield, ω_K, for Al ions with electron number $10 \leq N \leq 13$.

N	KLM/KLL			KMM/KLL			ω_K		
	HFR[a]	AS[b]	Rec[c]	HFR[a]	AS[b]	Rec[c]	HFR[a]	AS[b]	Rec[c]
10	0.023	0.021					0.0446	0.0467	
11	0.035	0.035		0.00021	0.00019		0.0445	0.0465	
12	0.042	0.045	0.042(6)	0.00068	0.00044	0.00044(12)	0.0425	0.0462	0.0387(12)
13	0.047	0.053		0.00066	0.00065		0.0424	0.0464	

Notes. [a] HFR calculation (this work). [b] AUTOSTRUCTURE calculation (this work). [c] Recommended value (Schönfeld & Janssen 1996).

Table 14. Al valence and K-vacancy levels with electron number $2 \leq N \leq 3$.

N	i	$2S+1$	L	$2J$	Conf.	E (keV)	$A_r(i)$ (s^{-1})	$A_a(i)$ (s^{-1})	$\omega_K(i)$
2	1	1	0	0	$1s^2\,^1S_0$	0.0000			
2	2	3	0	2	$1s2s\,^3S_1$	1.5745			
2	3	3	1	0	$1s2p\,^3P^o_0$	1.5874	1.37E+08		
2	4	3	1	2	$1s2p\,^3P^o_1$	1.5877	5.62E+10		
2	5	3	1	4	$1s2p\,^3P^o_2$	1.5884	1.71E+08		
2	6	1	0	0	$1s2s\,^1S_0$	1.5890	7.91E+02		
2	7	1	1	2	$1s2p\,^1P^o_1$	1.5983	2.99E+13		
3	1	2	0	1	$1s^22s\,^2S_{1/2}$	0.0000			
3	2	2	1	1	$1s^22p\,^2P^o_{1/2}$	0.0218	7.71E+08		
3	3	2	1	3	$1s^22p\,^2P^o_{3/2}$	0.0225	8.50E+08		
3	4	2	0	1	$1s2s^2\,^2S_{1/2}$	1.5567	1.53E+12	1.22E+14	0.012
3	5	4	1	1	$1s(^2S)2s2p(^3P^o)\,^4P^o_{1/2}$	1.5621	4.45E+09	2.00E+09	0.690
3	6	4	1	3	$1s(^2S)2s2p(^3P^o)\,^4P^o_{3/2}$	1.5624	1.17E+10	6.00E+09	0.661
3	7	4	1	5	$1s(^2S)2s2p(^3P^o)\,^4P^o_{5/2}$	1.5629	2.86E+03		1.000
3	8	2	1	1	$1s(^2S)2s2p(^3P^o)\,^2P^o_{1/2}$	1.5796	2.43E+13	8.94E+12	0.731
3	9	2	1	3	$1s(^2S)2s2p(^3P^o)\,^2P^o_{3/2}$	1.5800	2.55E+13	5.39E+12	0.825
3	10	4	1	1	$1s(^2S)2p^2(^3P)\,^4P_{1/2}$	1.5855	1.16E+10	1.00E+09	0.921
3	11	4	1	3	$1s(^2S)2p^2(^3P)\,^4P_{3/2}$	1.5858	1.36E+10	3.20E+10	0.298
3	12	4	1	5	$1s(^2S)2p^2(^3P)\,^4P_{5/2}$	1.5863	2.20E+10	2.22E+11	0.090
3	13	2	1	1	$1s(^2S)2s2p(^1P^o)\,^2P^o_{1/2}$	1.5881	3.36E+12	8.31E+13	0.039
3	14	2	1	3	$1s(^2S)2s2p(^1P^o)\,^2P^o_{3/2}$	1.5883	2.16E+12	8.67E+13	0.024
3	15	2	2	3	$1s(^2S)2p^2(^1D)\,^2D_{3/2}$	1.5971	1.37E+13	1.41E+14	0.088
3	16	2	2	5	$1s(^2S)2p^2(^1D)\,^2D_{5/2}$	1.5971	1.33E+13	1.43E+14	0.085
3	17	2	1	1	$1s(^2S)2p^2(^3P)\,^2P_{1/2}$	1.5998	4.12E+13	1.50E+10	1.000
3	18	2	1	3	$1s(^2S)2p^2(^3P)\,^2P_{3/2}$	1.6005	4.09E+13	1.91E+12	0.955
3	19	2	0	1	$1s(^2S)2p^2(^1S)\,^2S_{1/2}$	1.6130	1.24E+13	2.13E+13	0.369

Notes. This table is available in its entirety in its electronic form at the CDS. A portion is shown here for guidance regarding its form and content.

of Faenov et al. (1994), our calculated wavelengths for systems with $4 \leq N \leq 8$ were empirically shifted. Nonetheless, the quality of our HFR wavelengths for ions with $10 \leq N \leq 13$ is supported by comparisons with the laser-produced plasma experiment of Lecherbourg et al. (2007) and the data of Deslattes et al. (2003). Our HFR wavelengths agree with the HULLAC values (Behar & Netzer 2002) to within a few mÅ except for a few cases.

Regarding the radiative properties (A-values and radiative widths), our three calculations agree to within ~10% for values greater than 10^{13} s^{-1} if we exclude the decay properties of the Be-like and C-like levels $1s(^1S)2s2p^{2,4}(^2D,\,^4P)\,^3D_{1,2}$ and $^3P_{1,2}$ which are found to be sensitive to correlations with $n = 3$ configurations not considered in both of our AUTOSTRUCTURE and MCDF calculations. DHS and $1/Z$ radiative widths of Chen et al. (1981a,b, 1982) and Vainshtein & Safronova (1978), respectively, are found to be in reasonable accord with our three data sets for widths greater than or equal to 10^{13} s^{-1}, the others being more model dependent.

With regard to the Auger widths, good agreement is found between HFR and AUTOSTRUCTURE for values greater than 10^{13} s^{-1}, although the latter predicts slightly larger widths. As for the radiative widths, the DHS Auger widths computed by Chen et al. (1981a,b) for $N = 3, 7$ and the $1/Z$ theoretical values of Vainshtein & Safronova (1978) are in reasonable accord with our values that are greater than or equal to 10^{13} s^{-1}, and the others are more model dependent. HULLAC total widths (Behar & Netzer 2002) are systematically shorter by up to a factor of 2 or more than both our HFR and AUTOSTRUCTURE values. Comparisons of our predicted lifetimes with the available measurements (Armour et al. 1981; Buchet et al. 1984; Hellmann & Träbert 1985) have shown the importance of the two-body Breit interactions.

Our computed Kβ/Kα line ratios, KLM/KLL and KMM/KLL Auger channel ratios, and K-shell fluorescence yields have been compared with the recommended values of Schönfeld & Janssen (1996) for $N = 12$. The AUTOSTRUCTURE line ratio is within the error bar, with

Table 15. K-vacancy transitions in Al ions with electron number $2 \leq N \leq 3$.

N	k	i	λ (Å)	$A_r(k,i)$ (s^{-1})	$gf(i,k)$	CF
2	4	1	7.8091	5.61E+10	1.54E-03	-0.99
2	7	1	7.7574	2.99E+13	8.09E-01	-0.99
3	4	2	8.0779	5.35E+11	1.05E-02	0.55
3	4	3	8.0817	9.89E+11	1.94E-02	0.52
3	5	1	7.9369	4.45E+09	8.39E-05	-0.91
3	6	1	7.9354	1.17E+10	4.41E-04	-0.91
3	8	1	7.8491	2.43E+13	4.48E-01	-0.89
3	9	1	7.8472	2.54E+13	9.40E-01	-0.89
3	10	2	7.9290	9.50E+09	1.79E-04	0.85
3	10	3	7.9326	4.43E+08	8.36E-06	0.04
3	11	2	7.9274	1.06E+08	4.00E-06	-0.01
3	11	3	7.9310	1.18E+10	4.46E-04	0.93
3	12	3	7.9285	2.03E+10	1.15E-03	-0.88
3	13	1	7.8073	3.35E+12	6.12E-02	-0.11
3	14	1	7.8061	2.15E+12	7.85E-02	-0.08
3	15	2	7.8707	1.30E+13	4.84E-01	0.88
3	15	3	7.8742	6.44E+11	2.39E-02	-0.12
3	16	3	7.8739	1.33E+13	7.41E-01	0.88
3	17	2	7.8569	2.82E+13	5.22E-01	0.94
3	17	3	7.8605	1.30E+13	2.42E-01	-0.85
3	18	2	7.8536	4.94E+12	1.82E-01	0.51
3	18	3	7.8572	3.60E+13	1.33E+00	0.94
3	19	2	7.7920	3.40E+12	6.19E-02	0.55
3	19	3	7.7955	9.02E+12	1.64E-01	0.80

Notes. This table is available in its entirety in its electronic form at the CDS. A portion is shown here for guidance regarding its form and content. The wavelengths for $4 \leq N \leq 8$ have been empirically shifted (see the text).

MCDF just outside, and HFR is within 2 standard deviations. Our HFR KLM/KLL ratio is close to the Schönfeld & Janssen value, while the HFR KMM/KLL ratio is 2 standard deviations higher. In contrast, the AUTOSTRUCTURE KMM/KLL ratio is close to the recommended value. Although our HFR K-shell fluorescence yield is outside the error bar, the difference is less than 10%, while the discord with our AUTOSTRUCTURE value grows to 16%. Finally, the accuracy of our HFR Auger data is further supported by comparison of the experimental relative intensities of KLL Auger transitions obtained from the recent measurements of Huttula et al. (2009).

The present radiative and Auger widths will be used in the computation of the K-shell photoionization cross sections of these ions, which are required in XSTAR (Kallman & Bautista 2001) for modeling the interesting Al spectral features.

References

Armour, I. A., Silver, J. D., & Träbert, E. 1981, J. Phys. B, 14, 3563
Badnell, N. R. 1986, J. Phys. B, 19, 3827
Badnell, N. R. 1997, J. Phys. B, 30, 1
Bar-Shalom, A., Klapisch, M., & Oreg, J. 2001, J. Quant. Spectrosc. Radiat. Transfer, 71, 169
Bautista, M. A., & Kallman, T. R. 2001, ApJS, 134, 139
Bautista, M. A., Mendoza, C., Kallman, T. R., & Palmeri, P. 2003, A&A, 403, 339
Bautista, M. A., Mendoza, C., Kallman, T. R., & Palmeri, P. 2004, A&A, 418, 1171
Behar, E., & Netzer, H. 2002, ApJ, 570, 165
Buchet, J. P., Buchet-Poulizac, M. C., Denis, A., et al. 1984, J. Phys. (Paris) Lett., 45, L361
Deslattes, R. D., Kessler, E. G., Indelicato, P., et al. 2003, Rev. Mod. Phys., 75, 35
Chang, C., & Cui, W. 2007, ApJ, 663, 1207
Chen, M. H., Crasemann, B., Karim, K. R., & Mark, H. 1981a, Phys. Rev. A, 24, 1845
Chen, M. H., Crasemann, B., & Mark, H. 1981b, Phys. Rev. A, 24, 1852
Chen, M. H., Crasemann, B., & Mark, H. 1982, Phys. Rev. A, 26, 1441
Cowan, R. D. 1981, The Theory of Atomic Structure and Spectra (Berkeley: University of California Press)
Eissner, W., Jones, M., & Nussbaumer, H. 1974, Comput. Phys. Commun., 8, 270
Faenov, A. Ya., Pikuz, S. A., & Shlyaptseva, A. S. 1994, Phys. Scr., 49, 41
García, J., Mendoza, C., Bautista, M. A., et al. 2005, ApJS, 158, 68
García, J., Kallman, T. R., Witthoeft, M., et al. 2009, ApJS, 185, 477
Gorczyca, T. W., Kodituwakku, C. N., Korista, K. T., et al. 2003, ApJ, 592, 636
Grant, I. P., & McKenzie, B. J. 1980, J. Phys. B, 13, 2671
Grant, I. P., McKenzie, B. J., Norrington, P. H., Mayers, D. F., & Pyper, N. C. 1980, Comput. Phys. Commun., 21, 207
Hanke, M., Wilms, J., Nowak, M. A., et al. 2009, ApJ, 690, 330
Hellmann, H., & Träbert, E. 1985, Nucl. Instr. Meth. B, 9, 611
Holczer, T., Behar, E., & Arav, N. 2010, ApJ, 708, 981
Huenemoerder, D. P., Canizares, C. R., Drake, J. J., & Sanz-Forcada, J. 2003, ApJ, 595, 1131
Huttula, M., Partanen, L., Mäkinen, A., et al. 2009, Phys. Rev. A, 79, 023412
Kaastra, J. S., & Mewe, R. 1993, A&AS, 97, 443
Kallman, T., & Bautista, M. 2001, ApJS, 133, 221
Kallman, T. R., Palmeri, P., Bautista, M. A., Mendoza, C., & Krolik, J. H. 2004, ApJS, 155, 675
Kallman, T. R., Bautista, M. A., Goriely, S., et al. 2009, ApJ, 701, 865
Kaspi, S., Brandt, W. N., George, I. M., et al. 2002, ApJ, 574, 643
Lecherbourg, L., Renaudin, P., Bastiani-Ceccotti, S., et al. 2007, High Energy Density Phys., 3, 175
Loewenstein, M., & Davis, D. S. 2010, BAAS, 41, 483
McKenzie, B. J., Grant, I. P., & Norrington, P. H. 1980, Comput. Phys. Commun., 21, 233
Mendoza, C., Kallman, T. R., Bautista, M. A., & Palmeri, P. 2004, A&A, 414, 377
Nordon, R., & Behar, E. 2007, A&A, 464, 309
Ogle, P. M., Brookings, T., Canizares, C. R., Lee, J. C., & Marshall, H. L. 2003, A&A, 402, 849
Palmeri, P., Mendoza, C., Kallman, T. R., & Bautista, M. A. 2002, ApJ, 577, L119
Palmeri, P., Mendoza, C., Kallman, T. R., & Bautista, M. A. 2003a, A&A, 403, 1175
Palmeri, P., Mendoza, C., Kallman, T. R., Bautista, M. A., & Meléndez, M. 2003b, A&A, 410, 359
Palmeri, P., Quinet, P., Mendoza, C., et al. 2008a, ApJS, 177, 408
Palmeri, P., Quinet, P., Mendoza, C., et al. 2008b, ApJS, 179, 542
Peterson, J. R., Kahn, S. M., Paerels, F. B. S., et al. 2003, ApJ, 590, 207
Ralchenko, Y., Kramida, A. E., Reader, J., & NIST ASD Team. 2008, NIST Atomic Spectra Database, version 3.1.5 (Gaithersburg: NIST) http://physics.nist.gov/asd3
Schönfeld, E., & Janssen, H. 1996, Nucl. Instr. Meth. A, 369, 527
Schulz, N. S., Huenemoerder, D. P., Ji, L., et al. 2009, ApJ, 692, L80
Vainshtein, L. A., & Safronova, U. I. 1978, ADNDT, 21, 49
Watanabe, S., Sako, M., Ishida, M., et al. 2006, ApJ, 651, 421
Witthoeft, M. C., Bautista, M. A., Mendoza, C., et al. 2009, ApJS, 182, 127